Contents lists available at ScienceDirect

Biochemistry and Biophysics Reports

Bile acids induce Ca^{2+} signaling and membrane permeabilizations in vagal nodose ganglion neurons

Esmira Mamedova, Lív Bech Árting, Jens C. Rekling[*]

Department of Neuroscience, University of Copenhagen, Panum - 24.4, Blegdamsvej 3, DK-2200, Copenhagen N, Denmark

ARTICLE INFO

ABSTRACT

Bile acids (BAs) play an important role in the digestion of dietary fats and act as signaling molecules. However, due to their solubilizing properties, high concentrations in the gut may negatively affect gut epithelium and possibly afferent fibers innervating the gastrointestinal tract (GI). To determine the effect of BAs on intracellular Ca^{2+} and membrane permeabilization we tested a range of concentrations of two BAs on vagal nodose ganglion (NG) neurons, Chinese Hamster Ovary (CHO), and PC12 cell lines. NG explants from mice were drop-transduced with the genetically encoded Ca^{2+} indicator AAV9-Syn-jGCaMP7s and used to measure Ca^{2+} changes upon application of deoxycholic acid (DCA) and taurocholic acid (TCA). We found that both BAs induced a Ca^{2+} increase in NG neurons in a dose-dependent manner. The DCA-induced Ca^{2+} increase was dependent on intracellular Ca^{2+} stores. NG explants, with an intact peripheral part of the vagus nerve, showed excitation of NG neurons in nerve field recordings upon exposure to DCA. The viability of NG neurons at different BA concentrations was determined, and compared to CHO and PC12 cells lines using propidium iodide labeling, showing threshold concentrations of BA-induced cell death at 400–500 μM. These observations suggest that BAs act as Ca^{2+}-inducing signaling molecules in vagal sensory neurons at low concentrations, but induce cell death at higher concentrations, which may occur during inflammatory bowel diseases.

1. Introduction

Bile acids are widely known for their lipid solubilizing properties, however, they also perform an important role as signaling molecules throughout the body [1,2]. Hydrophobic BAs such as DCA and lithocholic acid (LCA) are cytotoxic at higher concentrations and can cause liver damage, lumen permeabilization, and are involved in neurological diseases [3]. Significantly increased levels of LCA, DCA, and TCA are detected in several brain disorders such as Alzheimer's disease, Parkinson's disease, and Multiple sclerosis [2,4]. Moreover, BAs can also act as tumor-promoting agents in a dose-dependent manner [5].

Several nuclear BAs receptors have been identified including farnesoid X receptor (FXR), vitamin D receptor (VDR), pregnane X receptor (PXR), and constitutive androstane receptor (CAR); and G protein-coupled receptors: Takeda G protein-coupled receptor 5 (TGR5), sphingosine-1-phosphate receptor 2 (S1PR2), and muscarinic acetylcholine receptor M3 (M3R) [6]. Activation of nuclear or membrane-bound BAs receptors modulates a variety of cellular processes which can affect a wide range of physiological functions [2].

A recent study has shown that DCA activates neurons through TGR5 in rat nodose ganglion *in vivo*. TGR5 is expressed on afferent terminals of the vagal nerve and activation of vagal TGR5 receptor may be involved in the transmission of satiety signals to the brain [7]. BAs might also be able of interacting with their receptors on vagal sensory neurons through systematic circulation [1,7,8].

The studies on high levels of BAs in several diseases have been conducted before [5,9,10]. However, little is known about the relation between physiological and pathological concentrations on vagal sensory neurons. Here, we used a genetically encoded Ca^{2+} sensor (GECI) and cell-death assays to study the effect of two BAs (DCA and TCA) on Ca^{2+} and cell viability in NG explants, CHO cells, and PC12 cells. We show that, depending on concentration, BAs can act as both – detergent or signaling molecules on vagal afferent cell bodies.

* Corresponding author.
E-mail address: jrekling@sund.ku.dk (J.C. Rekling).

2. Materials and methods

2.1. Ethical approval

All experiments and procedures were conducted in accordance with the protocols laid out by the Danish Ministry of Justice and the Danish National Committee for Ethics in Animal Research and the approval of the Department of Experimental Medicine at the Faculty of Health and Medical Sciences, University of Copenhagen.

2.1. NG explants

Medical Research Institute (NMRI) or C57BL/6J mice post-natal P21 to P30 days, of either sex, were euthanized by cervical dislocation. The nodose ganglions were ventrally dissected and transferred to chilled artificial cerebrospinal fluid (aCSF) containing (in mM): 138 NaCl, 4.5 KCl, 10 HEPES acid, 25 NaHCO3, 1.2 NaH2PO4, 1 D-Glucose, 1.2 MgCl2, 2.6 CaCl2; pH 7.4, equilibrated by bubbling with 95% O_2/5% CO_2. The cultures were kept in a sterile, humidified incubator at 35 °C, with 5% CO_2.

2.3. Viral transduction

Adeno-associated virus (AAV) construct containing genes for jGCaMP7s driven by the synapsin promoter [11] were obtained from Addgene - pGP-AAV-syn-jGCaMP7s-WPRE (AAV9, Addgene, Cat#:104487-AAV9, RRID:Addgene_104487). The virus was diluted in ultrapure water giving 3.3 x 10e12 vg/mL. NG explants were transduced by 1 μL drop application of diluted virus the next day after dissection and used for experiments after 5–25 days. Virally transduced NG explants were also used for enzymatic dissociation.

2.4. NG cell dissociation

Three to six NGs were enzymatically dissociated using 3 mg/mL Protease XXIII (Sigma-Aldrich P5380) and 10 units/mL Papain (Sigma-Aldrich, P4762). The ganglions were incubated with the enzymatic solution for 3 h at 35 °C. Enzymatic treatment was stopped by a wash with 1 mg/mL trypsin inhibitor (Sigma-Aldrich, T9253), following mechanical dissociation with a pipette of 250 μm diameter hole [12]. The cells were plated on poly-D-lysine coated cover glasses, placed in the incubator, and used for Ca^{2+} imaging after 4–14 days.

2.5. Ca²⁺ imaging

Ca^{2+} imaging of NG explants was recorded by a stereo microscope (Leica MZ16) and illuminated by an external light source for fluorescence excitation (Leica EL6000). Green channel fluorescence, for GECI, was visualized using a bandpass filter (GFP3: excitation: 470/40 nm, barrier filter 525/50 nm). Live image stacks were captured by an EMCCD camera (Andor Luca EM S DL-658 M, Andor Technology, Belfast, United Kingdom), controlled by the SOLIS software (Andor Technology, Belfast, United Kingdom). Fluorescence imaging of dissociated NG neurons was acquired using an inverse microscope (Zeiss -Axiovert 35), illuminated by Olympus U-RFL-T, and equipped with appropriate optical filters. Two bandpass filters were used, one to visualize GECI in the green channel (Chroma 41017: excitation bandpass 470/40 nm, emission bandpass 525/50 nm) and the other to visualize propidium iodide fluorescence in the red channel (TXR: excitation 560/40 nm, barrier filter 610 nm). Live image stacks were captured by an EMCCD camera (Andor Luca EM S DL-658 M, Andor Technology, Belfast, United Kingdom), controlled by the SOLIS software (Andor Technology, Belfast, United Kingdom). Imaging protocols employed 20x objective (ACH-ROPLAN 20x/0.45 Ph2). CCK-8 was used as a control in Ca^{2+} imaging experiments because CCKRs are abundantly expressed in NG neurons and has been previously shown to activate NG neurons [13], [14]. It is important to note that NG explants exhibit spontaneous Ca^{2+} activity, and in some neurons increase in Ca^{2+} can be observed at any time during data recording.

2.6. Nerve recording

Data from the recording pipette were digitally acquired in Igor Pro 8.04 64-bit program at a sampling rate of 5 Hz with a 2 kHz low-pass filter and 5 kHz high pass filter.

2.7. Drug application

For NG explants the drugs were applied by gravity flow for 10 min, whereas dissociated NG neurons were drug superfused for 4 min. All experiments were ended with a 55 mM KCl application. Drugs used in this study: CCK-8 (TOCRIS, Cat#: 1166), DCA sodium salt (Merck, Cat#: 264101), TCA sodium salt hydrate (Sigma-Aldrich, Cat#: 86339). Stock solutions of drugs were prepared in water. For bath applications drug stock solutions were added to aCSF. The flow was controlled by a SENSIRION flowmeter (SLF3S-1300F, Sensirion AG, Stafa, Switzerland).

2.8. Cell line cultures

PC12 cells were maintained in Dulbecco's modified Eagle's medium (DMEM) 1965 medium supplemented with 10% fetal bovine serum, 5% horse serum, 200 mM L-glutamine, 200 U/mL penicillin, and 5 μg/mL streptomycin. Chinese hamster ovary (CHO) cells were maintained in HAM F12 medium supplemented with 10% fetal bovine serum, 200 M L-glutamine, 200 U/mL penicillin, and 5 μg/mL streptomycin. Both cell lines were either cultured on a 100-mm Petri dish or a 96-well plate in an incubator at 35 °C with 5% CO_2.

2.9 Cell-death assays

Fluorescence and absorbance were measured on one 96-well plate at a time with a FLOUstar OPTIMA plate reader (BMG Labtech, Offenburg, Germany). The propidium iodide (PI) assay was performed as follows: the medium was removed from the wells and phosphate buffer, containing 23 mM NaH2PO4, and 77 mM Na2HPO4 with 1.5 μM PI was subsequently added to each well. DCA sodium salt or TCA sodium salt hydrate was added to the wells with a concentration gradient over the plate. The plate was read from the bottom with excitation/emission wavelengths of 544/615 nm. The readings were done 5, 10, and 20 min after adding the bile acids. Data were calculated as follows: the baseline was set as mean fluorescence values of the three lowest DCA and TCA concentrations. Max fluoresces (100%) was set to the highest. All values were normalized in this manner: (value-baseline)/(max – baseline) *100%.

The 3-(4,5-dimethylthiazol-2-yl)-2,5-diphenyltetrazolium bromide (MTT) assay was performed as follows: the medium was removed from the wells, and 50 μL of medium and 50 μL MTT (5 mg/mL) in PBS were added in each well. Subsequently, DCA sodium salt or TCA sodium salt was added as described above, incubated for 2 h at 35 °C. Before plate reading, PBS was exchanged for DMSO (AAT Bioquest, Cat#: 20052, Sunnyvale, CA, USA). The absorbance was read from above at OD = 590. The data calculations were performed as follows: the mean absorbance value of the three highest DCA concentrations was found, defined as no viability (0%). The baseline was set to the mean absorbance value of the four lowest DCA or TCA concentrations. Normalization of absorbance values was calculated by: (value – no viability)/(baseline – no viability) *100%.

2.10. Experimental design and statistical analysis

Recorded data were analyzed using ImageJ 1.53d (ImageJ, RRID: SCR_003070) and Igor Pro 8 (IGOR Pro, RRID:SCR_000325). All

statistical tests were carried out using GraphPad Prism 8 (RRID: SCR_002798). Data are reported as mean ± standard deviation (SD) unless otherwise noted. N = number of experiments and n = number of neurons.

The expression of jGCaMP7s in NG explants was used as a neuron selective marker to detect an increase in Ca2+ levels. Cells with low jGCaMP7s expression levels were excluded. For dissociated NG neurons Ca2+ response was defined as an amplitude of over 20 A U. Cells were excluded if the Ca2+ response to the drug was 50% higher than the KCl-induced Ca2+ transient.

Activity profiles for NG explants and somas/processes of dissociated NG neurons were measured in ImageJ. Some of the values from Ca2+ imaging were normalized to KCl. However, KCl was not used for normalization in experiments performed with Ca2+ free-ringer and EGTA or when measuring Ca2+ for a neuron in intact NG explant because of reflection from surrounding neurons.

Images with SMART or HiLo filters grouped for comparison have identical contrast settings.

3. Results

3.1. DCA increases vagus nerve activity and Ca²⁺ in NG explants

Recent developments in GECIs and viral transductions permit detailed analysis of Ca^{2+} dynamics in neurons ([11]). To investigate if BAs activate NG neurons, we used AAV9-Syn-jGCaMP7s transduced NG explants to perform Ca^{2+} imaging in the entire ganglion or nerve recording from a ganglion with part of the peripheral vagal nerve root intact (Fig. 1A). In addition, we used cultured dissociated NG neurons, pre-labeled with jGCaMP7s, for Ca^{2+} imaging in single neurons upon BAs applications.

To determine the effect of BAs on the electrical activity in NG neurons, the nerve-end of NG explants with part of the peripheral vagus nerve intact, was sucked into a recording pipette while the preparation was superfused with aCSF. Bath application of 500 µM DCA resulted in an increase in vagus nerve activity with an amplitude of 20 ± 6% of the nerve root response to 55 mM KCl (N = 3 NGs, Fig. 1B) confirming that the NG neurons are viable and excited by DCA when maintained in

explant culture.

Bath application of 250 µM DCA induced an increase in Ca^{2+} in NG explant neurons, and after a 20 min washout period, 10 nM CCK-8 induced an increase in Ca^{2+} in the same NG explant. The amplitude of the DCA response was 40 ± 20% of the CCK-8 response. (N = 3, Fig. 1C). The data from Ca^{2+} imaging in a dual-cultured NG experiment showed that 93 individual neurons responding to DCA were also responsive to CCK-8, indicating that the neurons were able to signal appropriately to CCK-8 after exposure to 250 µM DCA (Fig. 1C).

3.2. Concentration-dependent Ca²⁺ responses to DCA and TCA

Next, we examined whether two structurally different BA (DCA and TCA) induce a concentration-dependent Ca^{2+} increase in GECI-labeled NG explants and isolated NG neurons (Fig. 2). Firstly, we performed Ca^{2+} imaging on NG explants with increasing cumulative concentrations of bath-applied DCA or TCA, ranging from 25 µM to 800 µM, separated by 20 min wash periods. DCA induced Ca^{2+} transients during the 10 min application in a near-linear concentration-dependent manner increasing the fluorescence with ~4% pr. 100 µM increase (linear regression, $R^2 >$ 0.9, N = 4, Fig. 2A). A concentration-dependent increase in Ca^{2+} was also observed in NG explants upon TCA application above 25 µM, but these TCA-induced Ca^{2+} signals were smaller than the DCA-induced Ca^{2+} signals, with an increase of ~0.15% fluorescence pr. 100 µM TCA (linear regression, $R^2 = 0.9$, N = 4, Fig. 2B). In addition, whole-ganglion images of peak Ca^{2+} responses show wider and brighter areas of increased fluorescence at 400 µM DCA compared to 100 µM DCA, which was substantially smaller for TCA at the same concentrations (Fig, 2C). Peak TCA fluorescence in NG explants at both concentrations was more sparsely distributed, indicating different Ca^{2+} response patterns to DCA and TCA (Fig. 2D).

Secondly, we performed Ca^{2+} imaging in cultured dissociated NG neurons (Fig. 2E and F). Neurons attached to the cover glass were placed in the recording chamber, which was perfused with aCSF. DCA concentrations from 100 µM to 400 µM elevated Ca^{2+} in concentration-dependent fashion (n = 20, Fig. 2E). The Ca^{2+} increase upon adding 200 µM DCA was observed not only in the neuronal soma but also in fine processes projecting from the dissociated neurons (n = 24, Fig. 2F).
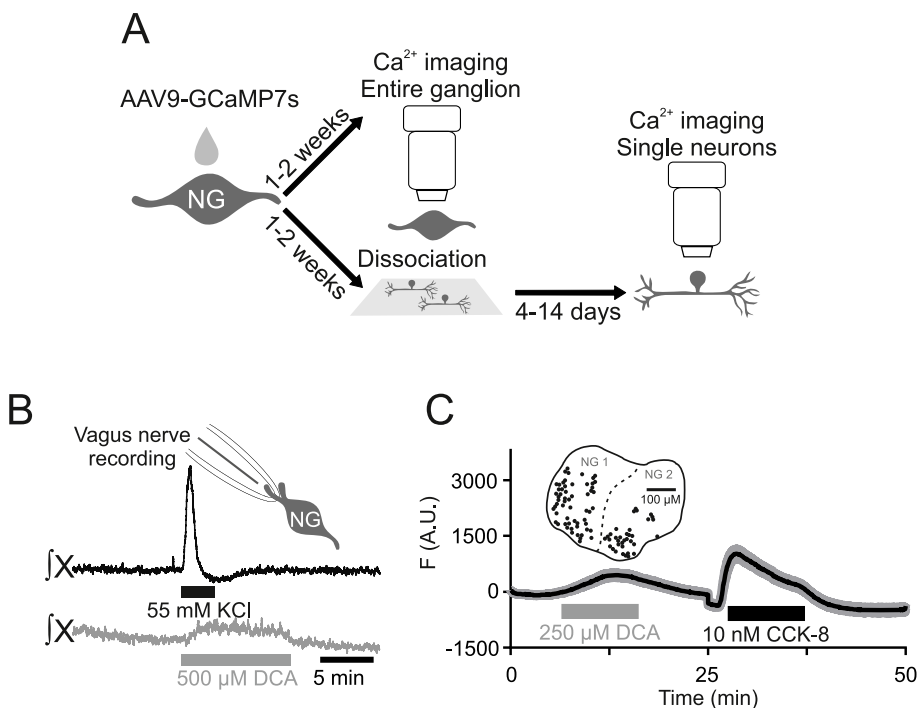
Fig. 1. DCA-induced increase in Ca^{2+} and field potential in NG explants. A, Representation of jGCaMP7s drop-transduced NG explant followed by entire ganglion or dissociated neurons Ca^{2+} imaging. B, Diagram shows NG explant with the peripheral part of vagus nerve, which was cut in half and sucked into the recording pipette before the experiment. Representative integrated vagal nerve (X) traces showing field potential increase upon application of 0.5 mM DCA (grey) and 55 mM KCl (black). C, Diagram representing two merged NG explants with selected neurons (n = 94 neurons). The graph shows the mean trace (black line) and the range of traces (grey) of jGCaMP7s labeled NG explants Ca^{2+} imaging upon application of 250 µM DCA followed by application of 10 nM CCK-8.
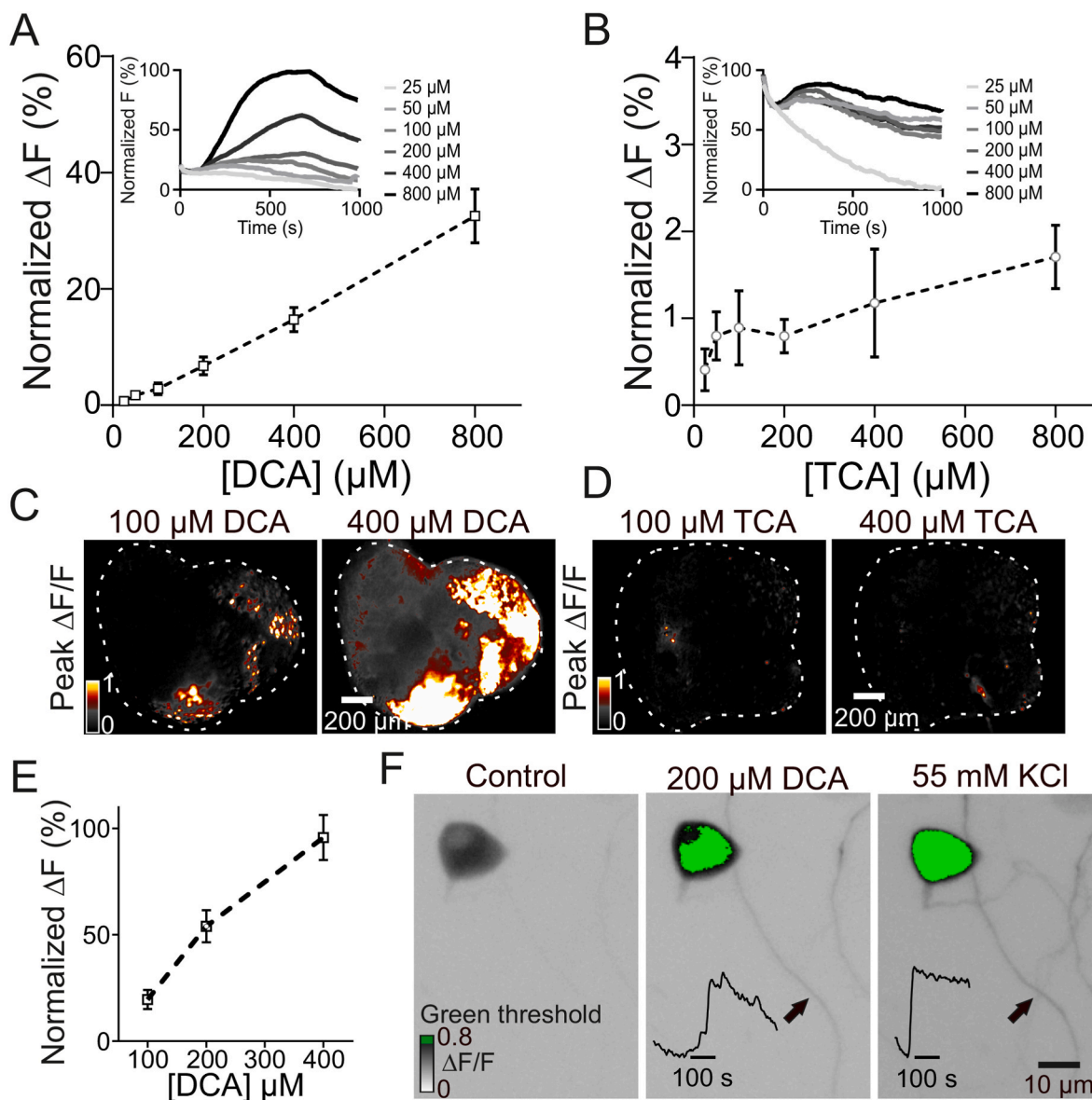
Fig. 2. Dose-dependent BA-induced increase in cytosolic Ca^{2+} in NG explants and dissociated NG neurons. A, B, Response profiles of DCA and TCA-induced Ca^{2+} increase at different concentrations. The DCA and TCA responses are normalized to the KCl-induced Ca^{2+} response amplitudes (data show: mean $\pm$ SEM, N = 4). Inserts: representative traces of DCA and TCA-dependent Ca^{2+} increase. Values are normalized in relation to min and max fluorescence for a single DCA or TCA cumulative dose experiment. C, D, Representative images of Ca^{2+} imaging of jGCaMP7s labeled NG explants upon bath application of 100 μM and 400 μM DCA and TCA, respectively. The dotted line outlines NG explants (2 pr. image); the calibration bar indicates the relative fluorescence ratio with the highest Ca^{2+}. E, Average Ca^{2+} response amplitudes to bath applied DCA (100 μM, 200 μM, and 400 μM) for single NG neurons labeled with jGCaMP7s (data show mean $\pm$ SEM, n $\geq$ 8). F, Representative image of isolated NG neuron labeled with jGCaMP7s before DCA application (control) and Ca^{2+} increase in the soma and neurites upon application of 200 μM DCA and 55 mM KCl. The traces in the images present Ca^{2+} transient in neurites (the arrow shows the measurement site); green in the calibration bar indicates values above 0.8. The DCA responses are normalized to KCl-induced Ca^{2+} response amplitudes. (For interpretation of the references to colour in this figure legend, the reader is referred to the Web version of this article.)

3.3. DCA elevates intracellular Ca^{2+} in a subset of NG neurons and likely involves intracellular Ca^{2+} stores

The following experiments were performed to explore whether all or a subset of NG neurons respond to DCA, and investigate where the DCA-induced Ca^{2+} increase originates from. A responder neuron was defined as a neuron with an evoked Ca^{2+} response at the soma with an amplitude of over 20 A U. In a standard aCSF 64% of tested neurons responded to 200 μM DCA with a Ca^{2+} transient amplitude of 72 $\pm$ 23% of KCl amplitude (n = 14, Fig. 3A), whereas all tested neurons responded to 400 μM DCA, with a Ca^{2+} transient amplitude of 82 $\pm$ 29% (n = 8, Fig. 3B).

Next, we removed extracellular Ca^{2+} from standard aCSF and added 1 mM EGTA 1 min prior to DCA application [15]. In the absence of extracellular Ca^{2+}, 64% percent of tested neurons responded to 200 μM and gave a Ca^{2+} amplitude of 80 $\pm$ 103 A U. (n = 28, Fig. 3C).

Subsequently, we depleted intracellular Ca^{2+} stores by a 30 min preincubation with 100 nM thapsigargin, an irreversible SERCA inhibitor [16]. The efficiency of pre-incubating dissociated NG neurons with thapsigargin was tested by caffeine application. Caffeine-induced cytosolic Ca^{2+} increase in Ca^{2+} free aCSF was abolished after thapsigargin pre-incubation (n = 10, not shown), confirming that ER stores were emptied by this procedure [17].

33% of dissociated NG neurons pre-incubated with thapsigargin
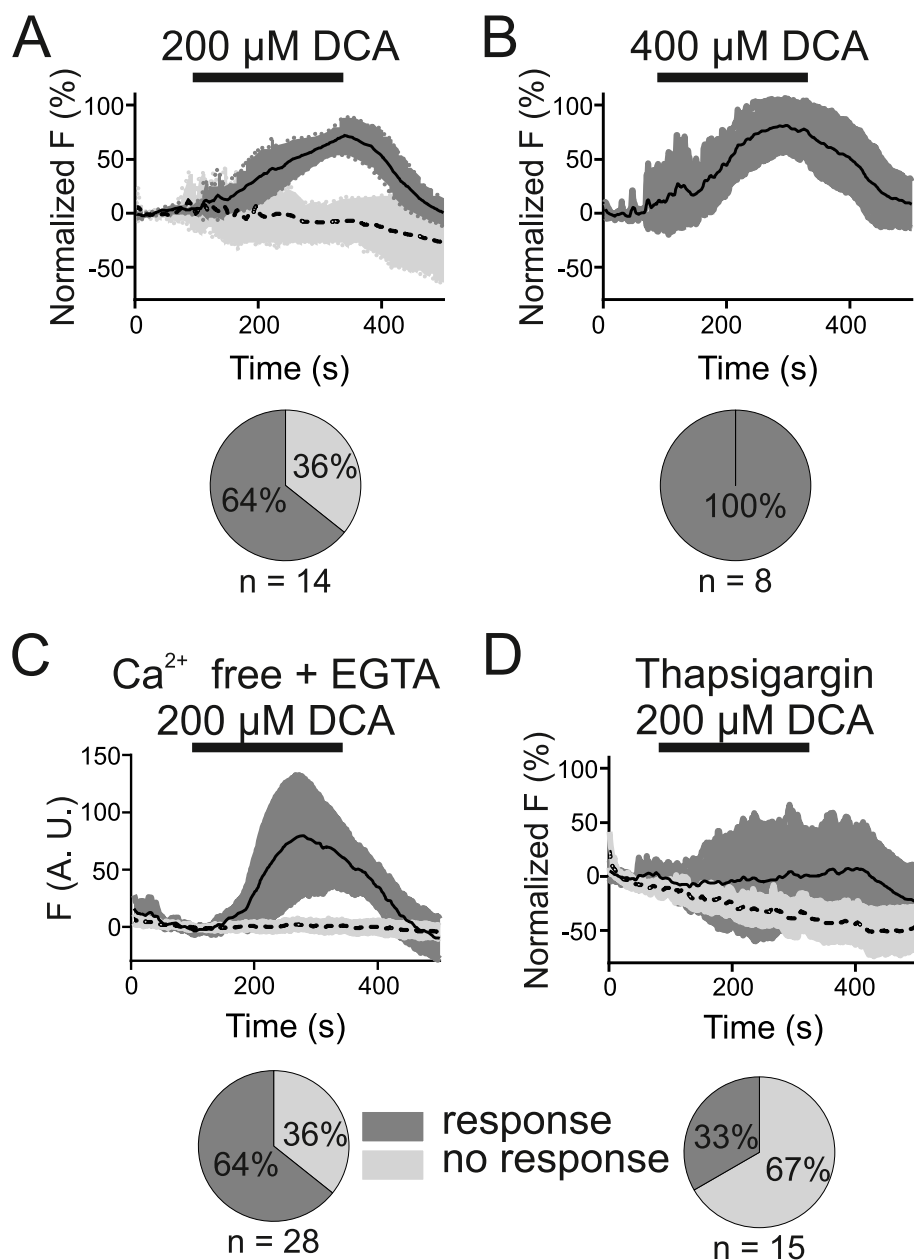
Fig. 3. Ca^{2+} imaging of dissociated NG neurons expressing jGCaMP7s: DCA-induced Ca^{2+} signal in standard aCSF, Ca^{2+} free aCSF, and with no Ca^{2+} gradient between cytosol, and endoplasmic reticulum. A, B, Average traces represent Ca^{2+} response (dark grey) or no response (light grey) to 200 μM and 400 μM DCA in standard aCSF, respectively. C, Average traces represent Ca^{2+} response (dark grey) or no response (light grey) to 200 μM DCA in Ca^{2+} free aCSF + 1 μM EGTA. D, Average traces represent Ca^{2+} response (dark grey) or no response (light grey) to 200 μM DCA in NG neurons where ER stores were depleted by incubation with 100 nM TG. In graphs, average traces represent Ca^{2+} traces (black line) and the corresponding 95% confidence interval (grey) upon application of DCA. Pie graphs indicate relative responsive neurons within each tested condition.

responded to 200 μM DCA with a Ca^{2+} amplitude of 4 ± 32% (n = 15, Fig. 3D). It can be noted that response and no-response traces have overlapping 95% confidence intervals.

3.4. DCA-induced cell death

Next, we examined if DCA and TCA can cause concentration-dependent cell membrane permeabilization leading to cell death in NG neurons. PI staining of dissociated jGCaMP7s-labeled NG neurons was determined before and after DCA application. At 100 μM DCA the morphology of neurons did not change, however at 500 μM DCA the neurons were significantly affected, showing truncated processes and swollen somas. The difference in soma area was measured, showing that 100 μM DCA did not change the soma size (−7% ± 5%), whereas 500 μM DCA increased the soma size by 60 ± 25% (unpaired *t*-test, p < 0.0001, n = 10, Fig. 4A).

Following, different DCA concentrations ranging from 100 to 500 μM were tested in PI-labeled dissociated NG neurons to identify a threshold

concentration for DCA-induced cell death. No changes in fluorescence intensity were observed upon 100–300 μM DCA, however, PI fluorescence increased at 400 μM DCA in some cells. A significant increase in fluorescence was seen at 500 μM DCA, however, 500 μM TCA did not enhance PI fluorescence, demonstrating that TCA does not cause cell membrane permeability at this concentration (p < 0.0001 for 500 μM DCA, p = 0.9192 for 500 μM TCA, Ordinary one-way ANOVA with multiple comparisons, n = 11).

In addition, we tested whether exposure to DCA is pathological in other cell lines and has a general membrane permeabilizing effect. The PI assay was performed on CHO and neuronal-like PC12 cells. Incubation of PI–labeled cells with DCA concentrations between 0.4 μM–4 mM resulted in enhanced fluorescence intensity at higher DCA concentrations (Fig. 4C), with an EC50 value of 0.47 mM for CHO cells and 0.59 mM for PC12 cells (non-linear regression, n = 4 wells). In contrast, incubation of CHO and PC12 cell lines with TCA did not show changes in PI fluorescence (Fig. 4C).

Finally, an MTT assay was conducted to determine the BA effect on
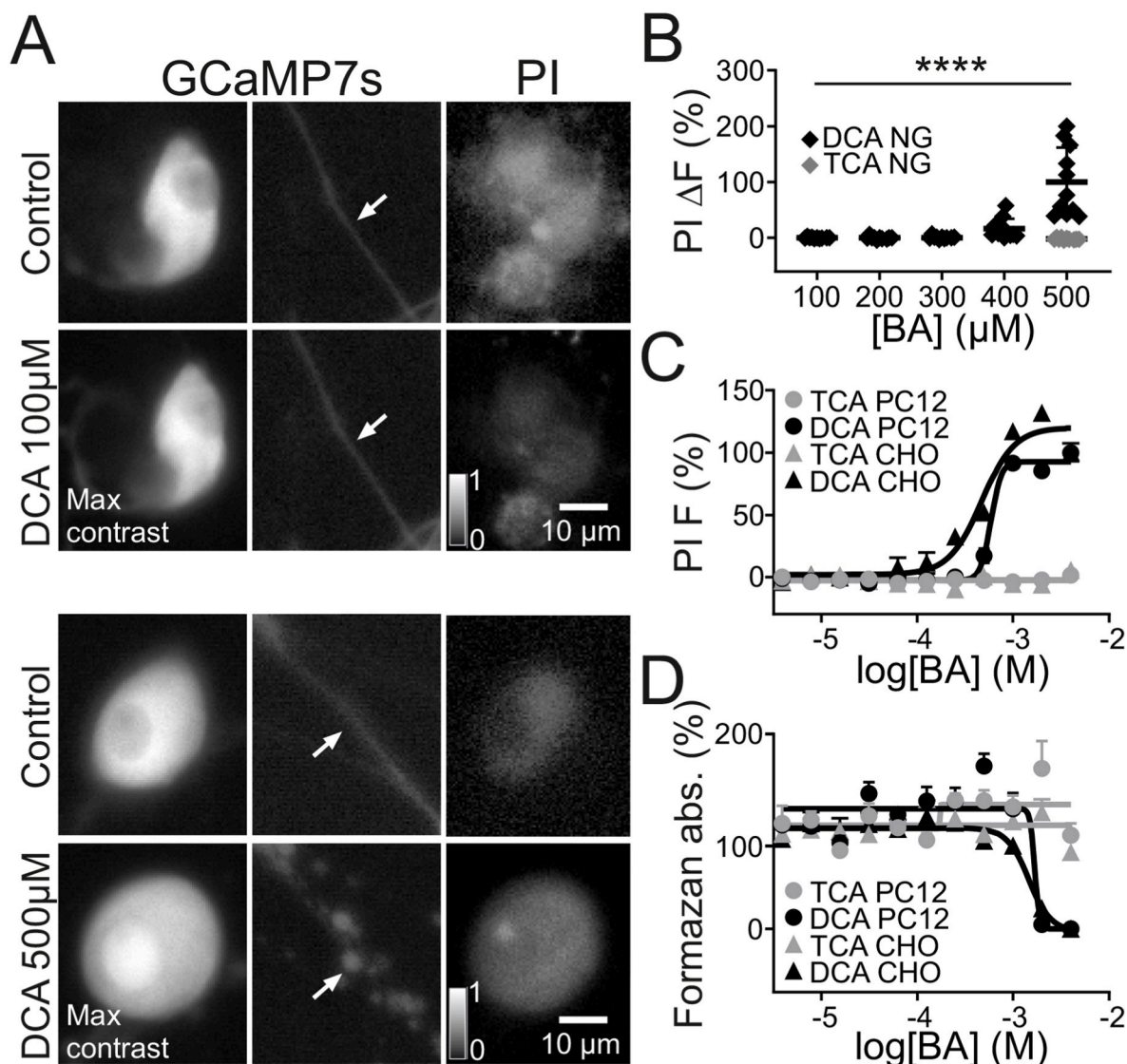
Fig. 4. Bile acid-induced cell death. A, Images of jGCaMP7s labeled somas and processes (white arrows) of dissociated NG neurons. PI labeled NG neurons before DCA application (control) and after 100 μM DCA (top panel) and 500 μM DCA (bottom panel); calibration bars indicate relative fluorescence intensity. B, Effect of DCA and TCA on NG neuron membrane permeability. Change of PI fluorescence intensity after 4 min bath applied DCA ($p < 0.0001$ for 500 μM DCA, $p = 0.9192$ for 500 μM TCA, Ordinary one-way ANOVA with multiple comparisons, n = 11). C, Effect of DCA and TCA on membrane permeability for CHO and PC12 cells. PI assay – PI fluorescence intensity after incubation with DCA and TCA, normalized to max fluorescence for each cell strain (n = 4 wells). D, Effect of DCA and TCA on CHO and PC12 cells viability. MTT assay – formazan absorbance after DCA or TCA incubation. Normalized by setting 100% as a baseline at the three lowest bile acid concentrations and 0% to the lowest absorbance for each cell strain (n = 4 wells). Log [BA] (M) indicate concentration range of 0.004–4 mM for DCA and TCA.

cell viability and cytotoxicity. In accordance with previous experiments, the higher concentrations of DCA decreased cell viability, which was not the case for TCA (Fig. 4D). The analysis of DCA data showed EC50 of 1.5 mM and 1.7 mM for CHO and PC12, respectively (non-linear regression, n = 4 wells).

4. Discussion

In a normal physiological state, BAs concentrations in human plasma are fluctuating between 5 μM and 15 μM [18,19]. In pathophysiological conditions such as irritable bowel syndrome (IBS), DCA levels in the colon can reach up to 1 mM. In the case of leaky gut syndrome, the gap junctions between intestinal enterocytes are disrupted, therefore there could be some spillover of DCA from the intestinal content. Since vagal afferents are closely located to EECs, there could be some direct effect of high DCA concentrations on vagal fiber endings [20]. Reports show that BAs levels above 1.5 mM can damage blood-brain barrier (BBB) due to

their detergent-like properties. However, in a range of 0.2 mM–1.5 mM they can affect lipid bilayers more subtly by modifying their structure [21]. DCA and chenodeoxycholic acid (CDCA) can interact with gap junctions proteins, leading to a leaky BBB [1]. A case study has also shown that a patient with hypercholanemia had drastically elevated BA levels in plasma reaching up to 1.5 mM [22]. Another study has demonstrated that bile duct ligation increased BA levels above 400 μM in the circulation the first day after the surgery [23]. In the present study, we combined Ca^{2+} imaging, *in vitro* vagus nerve recordings, and cell-death assays and showed that concentrations below 400–500 μM DCA and TCA induce Ca^{2+} signaling, dependent on intracellular Ca^{2+} stores, but DCA concentrations above that are cytotoxic to NG neurons by causing membrane permeabilization.

A recent study demonstrated that intra-arterial administration of DCA induced vagal afferent firing in the rat *in vivo* in single-unit NG recordings [7]. We chose to investigate the effects of primary conjugated bile acid TCA and secondary bile acid DCA in mice vagal NG neurons.

DCA is a more hydrophobic molecule than TCA, and that could be a reason that the concentration threshold for inducing cell permeabilization and consequent cell death showed to be different for these two BAs [24]. We identified that at higher concentrations DCA starts acting more like a cell membrane solubilizing agent than a signaling molecule. Our study showed that DCA and TCA have different properties on cell permeabilization and signaling.

In the dose-response experiments, the TCA-induced Ca^{2+} signal in NG explants was 25 fold lower than the DCA-induced Ca^{2+} signal (Fig. 2A and B). DCA is known as an agonist for TGR5 whereas TCA most likely activates S1PR2 which has been shown to bind conjugated BAs [25–28]. Additionally, BAs can activate acetylcholine muscarinic receptors and MAS related GPR family Member X4 (MRGPRX4) [29–32]. Recent single-cell sequencing data showed that Sphingosine-1-phosphate, muscarinic acetylcholine receptors, and MAS-related GPR family receptors are expressed in NG neurons, therefore Ca^{2+} responses upon applications of BAs could be due to activation of these receptors [13,33]. DCA binding to TGR5 induces signaling via the Gs pathway which leads to a rise in intracellular cAMP levels [26]. It has been also found that elevated cAMP in cortical neurons and astrocytes increased intracellular Ca^{2+} concentrations which may be mediated by activation of TGR5 [34]. Moreover, BAs induce ATP release which, in turn, activates purinergic receptors followed by a Ca^{2+} increase. In this activation pathway, TGR5 receptors are not involved [35]. Interestingly, BA receptor MRGPRX4 demonstrated 20 fold higher affinity for DCA compared to TCA, indicating a structure-affinity relationship for BAs [36,37]. Further studies are needed to elucidate novel mechanisms of DCA-induced Ca^{2+} increase in NG neuron populations.

We aimed to investigate the origin of Ca^{2+} upon exposure to DCA. Bath applications of DCA in standard aCSF and Ca^{2+} free aCSF showed the same results where 64% of tested NG neurons responded, indicating that Ca^{2+} was released from intracellular stores. When NG neurons were incubated with thapsigargin to empty intracellular Ca^{2+} stores, the Ca^{2+} increase upon DCA application in aCSF was still observed in 33% of NG neurons, showing that DCA-induced Ca^{2+} increase might be an influx of extracellular Ca^{2+} or come from other intracellular stores such as mitochondria.

Finally, we investigated which concentrations are lethal to dissociated NG neurons. The application of 500 μM DCA on dissociated PI labeled neurons induced cell death, whereas, the same concentration of TCA did not affect neurons. This led us to explore if other cell lines are similarly affected by high BAs concentration. Cell death and viability assays showed that at high concentrations DCA has a general permeabilizing effect on several cell lines including NG neurons, neuron-like, and cancer cell lines. This finding can also be supported by the physicochemical properties of these two BAs [38–40]. Taurine conjugated BAs are less hydrophobic and thus should not be membrane permeable. This suggests that TCA could only interact with membrane receptors, whereas DCA is able of entering cells due to its more hydrophobic structure [27]. Based on the PI cell death assay, we propose, that the DCA permeabilizing effect on dissociated NG neurons begins at 400 μM, inducing a partial disruption of the cell membrane lipid layer due to detergent and lytic actions causing influx of extracellular Ca^{2+}, which subsequently can lead to cell apoptosis. Additionally, the MTT assay performed on PC12 and CHO cells gave higher EC50 values with DCA incubation than the PI assay suggesting that cell death is likely caused by membrane permeabilization. At slightly lower than critical concentrations DCA may reversibly permeabilize cell membranes by interacting with the lipid layers, whereas above the threshold concentrations DCA may induce permanent holes in the cell membranes.

Further studies are needed to identify which receptors are involved in DCA- and TCA-induced signaling. This could be achieved by using TGR5 or S1PR2 knockout neurons or RNA silencing techniques.

5. Conclusion

In summary, we demonstrated that two BAs DCA and TCA induce different Ca^{2+} signals and have distinct properties for BA-induced cell permeabilization. Our results suggest that at lower concentrations DCA may act as a signaling molecule on vagal NG neurons, however, at higher concentrations, it can lead to cell death, which may contribute to pathological changes in several inflammatory bowel diseases [41].

Declaration of competing interest

All authors declare no conflicts of interest.

Acknowledgements

Appendix A. Supplementary data

Supplementary data to this article can be found online at https://doi.org/10.1016/j.bbrep.2022.101288.

References

[1] K.L. Mertens, et al., Bile acid signaling pathways from the enterohepatic circulation to the central nervous system, Front. Neurosci. 11 (2017) 617.
[2] M. McMillin, S. DeMorrow, Effects of bile acids on neurological function and disease, Faseb. J. 30 (11) (2016) 3658–3668.
[3] S. Wei, X. Ma, Y. Zhao, Mechanism of hydrophobic bile acid-induced hepatocyte injury and drug discovery, Front. Pharmacol. 11 (2020) 1084.
[4] P. Bhargava, et al., Bile acid metabolism is altered in multiple sclerosis and supplementation ameliorates neuroinflammation, J. Clin. Invest. 130 (7) (2020) 3467–3482.
[5] S. Jean-Louis, et al., Deoxycholic acid induces intracellular signaling through membrane perturbations, J. Biol. Chem. 281 (21) (2006) 14948–14960.
[6] A.L. Ticho, et al., Bile acid receptors and gastrointestinal functions, Liver Res. 3 (1) (2019) 31–39.
[7] X. Wu, et al., Satiety induced by bile acids is mediated via vagal afferent pathways, JCI Insight 5 (14) (2020).
[8] T.M.Z. Waise, H.J. Dranse, T.K.T. Lam, The metabolic role of vagal afferent innervation, Nat. Rev. Gastroenterol. Hepatol. 15 (10) (2018) 625–636.
[9] Z. Wang, et al., (-)-Epicatechin and NADPH oxidase inhibitors prevent bile acid-induced Caco-2 monolayer permeabilization through ERK1/2 modulation, Redox Biol. 28 (2020) 101360.
[10] M.P. Taranto, G. Perez-Martinez, G. Font de Valdez, Effect of bile acid on the cell membrane functionality of lactic acid bacteria for oral administration, Res. Microbiol. 157 (8) (2006) 720–725.
[11] H. Dana, et al., High-performance calcium sensors for imaging activity in neuronal populations and microcompartments, Nat. Methods 16 (7) (2019) 649–657.
[12] A. Saunders, et al., Molecular diversity and specializations among the cells of the adult mouse brain, Cell 174 (4) (2018) 1015–1030, e16.
[13] J. Kupari, et al., An atlas of vagal sensory neurons and their molecular specialization, Cell Rep. 27 (8) (2019) 2508–2523 e4.
[14] S.M. Simasko, et al., Cholecystokinin increases cytosolic calcium in a subpopulation of cultured vagal afferent neurons, Am. J. Physiol. Regul. Integr. Comp. Physiol. 283 (6) (2002) R1303–R1313.
[15] R.H. Kramer, R. Mokkapatti, E.S. Levitan, Effects of caffeine on intracellular calcium, calcium current and calcium-dependent potassium current in anterior pituitary GH3 cells, Pflügers Archiv 426 (1–2) (1994) 12–20.
[16] J.S. Hooper, et al., Store-operated calcium entry in vagal sensory nerves is independent of Orai channels, Brain Res. 1503 (2013) 7–15.
[17] M. Henrich, K.J. Buckler, Cytosolic calcium regulation in rat afferent vagal neurons during anoxia, Cell Calcium 54 (6) (2013) 416–427.
[18] E.A. Shaffer, E.R. Gordon, Serum bile acids as related to bile acid secretion in liver disease, Am. J. Dig. Dis. 23 (5) (1978) 392–397.
[19] T. Sugita, et al., Analysis of the serum bile Acid composition for differential diagnosis in patients with liver disease, Gastroenterol Res. Pract. 2015 (2015) 717431.
[20] Y. Yu, et al., Deoxycholic acid activates colonic afferent nerves via 5-HT3 receptor-dependent and -independent mechanisms, Am. J. Physiol. Gastrointest. Liver Physiol. 317 (3) (2019) G275–G284.
[21] J. Greenwood, et al., The effect of bile salts on the permeability and ultrastructure of the perfused, energy-depleted, rat blood-brain barrier, J. Cerebr. Blood Flow Metabol. 11 (4) (1991) 644–654.
[22] S.J. Karpen, P.A. Dawson, Not all (bile acids) who wander are lost: the first report of a patient with an isolated NTCP defect, Hepatology 61 (1) (2015) 24–27.

[23] M. Quinn, et al., Bile acids permeabilize the blood brain barrier after bile duct ligation in rats via Rac1-dependent mechanisms, Dig. Liver Dis. 46 (6) (2014) 527–534.

[24] N.I. Hanafi, et al., Overview of bile acids signaling and perspective on the signal of ursodeoxycholic acid, the most hydrophilic bile acid, in the heart, Biomolecules 8 (4) (2018).

[25] T. Maruyama, et al., Identification of membrane-type receptor for bile acids (M-BAR), Biochem. Biophys. Res. Commun. 298 (5) (2002) 714–719.

[26] Y. Kawamata, et al., A G protein-coupled receptor responsive to bile acids, J. Biol. Chem. 278 (11) (2003) 9435–9440.

[27] H. Duboc, Y. Tache, A.F. Hofmann, The bile acid TGR5 membrane receptor: from basic research to clinical application, Dig. Liver Dis. 46 (4) (2014) 302–312.

[28] B.L. Copple, T. Li, Pharmacology of bile acid receptors: evolution of bile acids from simple detergents to complex signaling molecules, Pharmacol. Res. 104 (2016) 9–21.

[29] S. Fiorucci, E. Distrutti, Bile acid-activated receptors, intestinal microbiota, and the treatment of metabolic disorders, Trends Mol. Med. 21 (11) (2015) 702–714.

[30] J.P. Raufman, K. Cheng, P. Zimniak, Activation of muscarinic receptor signaling by bile acids: physiological and medical implications, Dig. Dis. Sci. 48 (8) (2003) 1431–1444.

[31] E. Ibrahim, et al., Bile acids and their respective conjugates elicit different responses in neonatal cardiomyocytes: role of Gi protein, muscarinic receptors and TGR5, Sci. Rep. 8 (1) (2018) 7110.

[32] S.H. Sheikh Abdul Kadir, et al., Bile acid-induced arrhythmia is mediated by muscarinic M2 receptors in neonatal rat cardiomyocytes, PLoS One 5 (3) (2010) e9689.

[33] K.L. Egerod, et al., Profiling of G protein-coupled receptors in vagal afferents reveals novel gut-to-brain sensing mechanisms, Mol. Metabol. 12 (2018) 62–75.

[34] V. Keitel, et al., The bile acid receptor TGR5 (Gpbar-1) acts as a neurosteroid receptor in brain, Glia 58 (15) (2010) 1794–1805.

[35] J.M. Kowal, et al., Bile acid effects are mediated by ATP release and purinergic signalling in exocrine pancreatic cells, Cell Commun. Signal. 13 (2015) 28.

[36] T.W. Pols, et al., The bile acid membrane receptor TGR5 as an emerging target in metabolism and inflammation, J. Hepatol. 54 (6) (2011) 1263–1272.

[37] H. Yu, et al., MRGPRX4 Is a Bile Acid Receptor for Human Cholestatic Itch, vol. 8, Elife, 2019.

[38] M.J. Perez, O. Briz, Bile-acid-induced cell injury and protection, World J. Gastroenterol. 15 (14) (2009) 1677–1689.

[39] R. Schubert, K.H. Schmidt, Structural changes in vesicle membranes and mixed micelles of various lipid compositions after binding of different bile salts, Biochemistry 27 (24) (1988) 8787–8794.

[40] V. Urdaneta, J. Casadesus, Interactions between bacteria and bile salts in the gastrointestinal and hepatobiliary tracts, Front. Med. 4 (2017) 163.

[41] J.P. Thomas, et al., The emerging role of bile acids in the pathogenesis of inflammatory bowel disease, Front. Immunol. 13 (2022) 829525.